Supporting information

La@[La5&B30] 0/–/2–: Endohedral Trihedral Metallo-Borospherenes With Spherical Aromaticity

Mei-Zhen Ao,[a,b] Xiao-Qin Lu,[a] Wen-Yan Zan, *[a] Yue-Wen Mu,*[a] and Si-Dian Li*[a]
[a]*Nanocluster Laboratory, Institute of Molecular Science Shanxi University, Taiyuan 030006, P.R. China.*
[b]*Fenyang College of Shanxi Medical University, Fenyang 032200, China*
**E-mail: zanwy@sxu.edu.cn, ywmu@sxu.edu.cn and lisidian@sxu.edu.cn*

Table of Contents

La@[La_5&B_{30}]$^-$ (**2**), and (b) C_6H_6 based on their calculated NICS-ZZ components.

Table S1. Optimized coordinates (x, y, z) of D_{3h} La@[La_5&B_{30}] (**1**, $^3A_1'$) at PBE0 level.

Table S2. Optimized coordinates (x, y, z) of C_s La@[La_5&B_{30}]$^-$ (**2**, $^2A'$) at PBE0 level.

Table S3. Optimized coordinates (x, y, z) of D_{3h} La@[La_5&B_{30}]$^{2-}$ (**3**, $^1A_1'$) at PBE0 level.

Table S4. Optimized fractional coordinates (x, y, z) of 1D La_4B_{21} (**4**) nanowire.

Figure S1. Relative energies of the thirty lowest-lying isomers of La_6B_{30} at PBE0, TPSSh (parentheses) and CCSD(T) (square brackets) levels in eV.

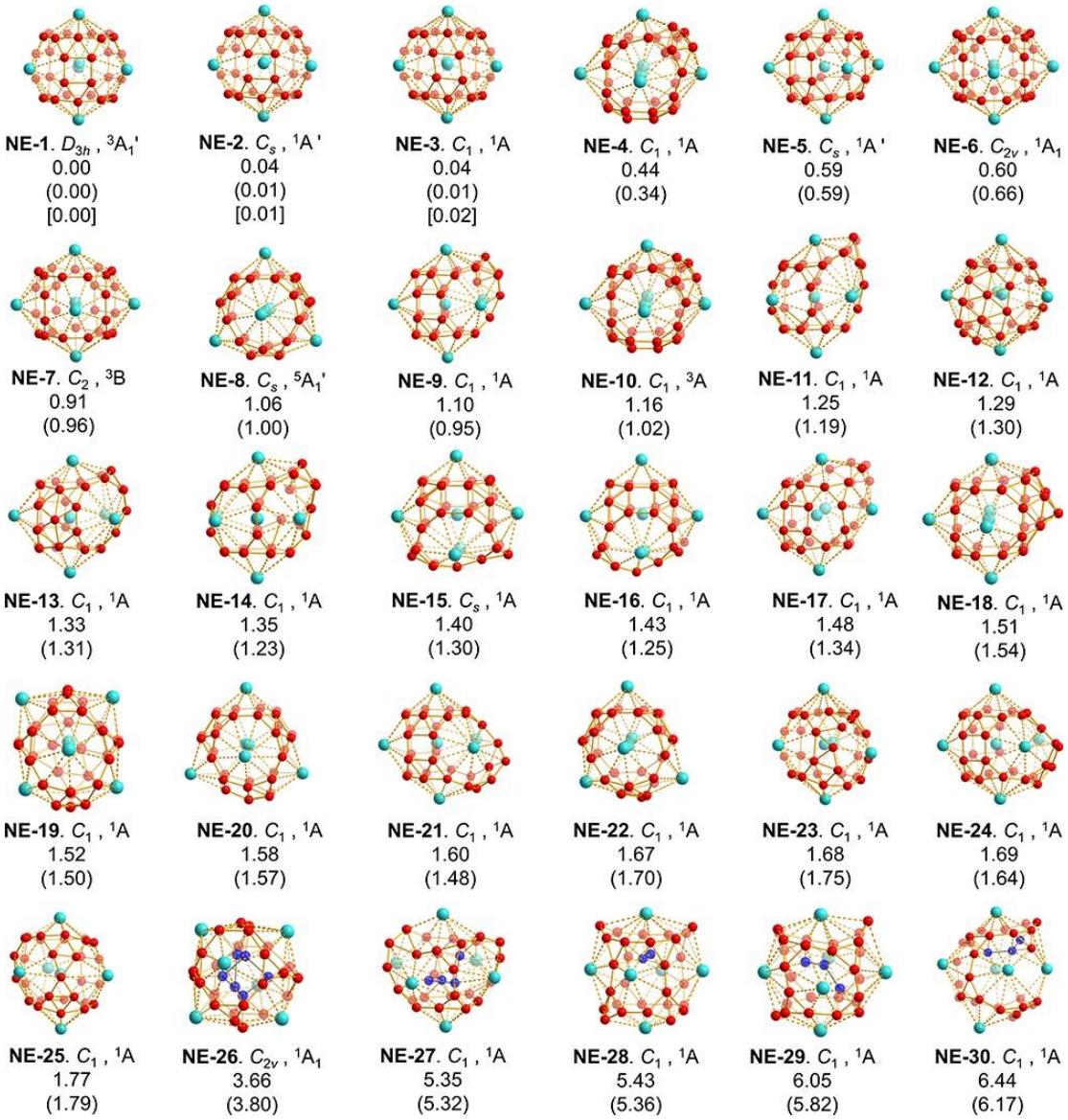

Figure S2. Relative energies of the twelve lowest-lying isomers of $La_6B_{30}^-$ at PBE0 and TPSSh (parentheses) level in eV.

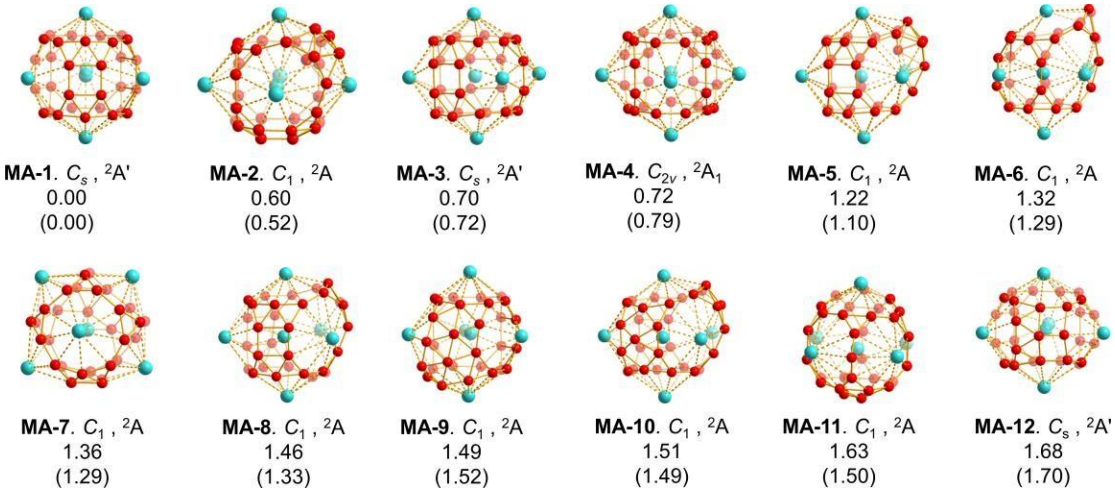

Figure S3. Relative energies of the eighteen lowest-lying isomers of $La_6B_{30}^{2-}$ at PBE0 and TPSSh (parentheses) level in eV.

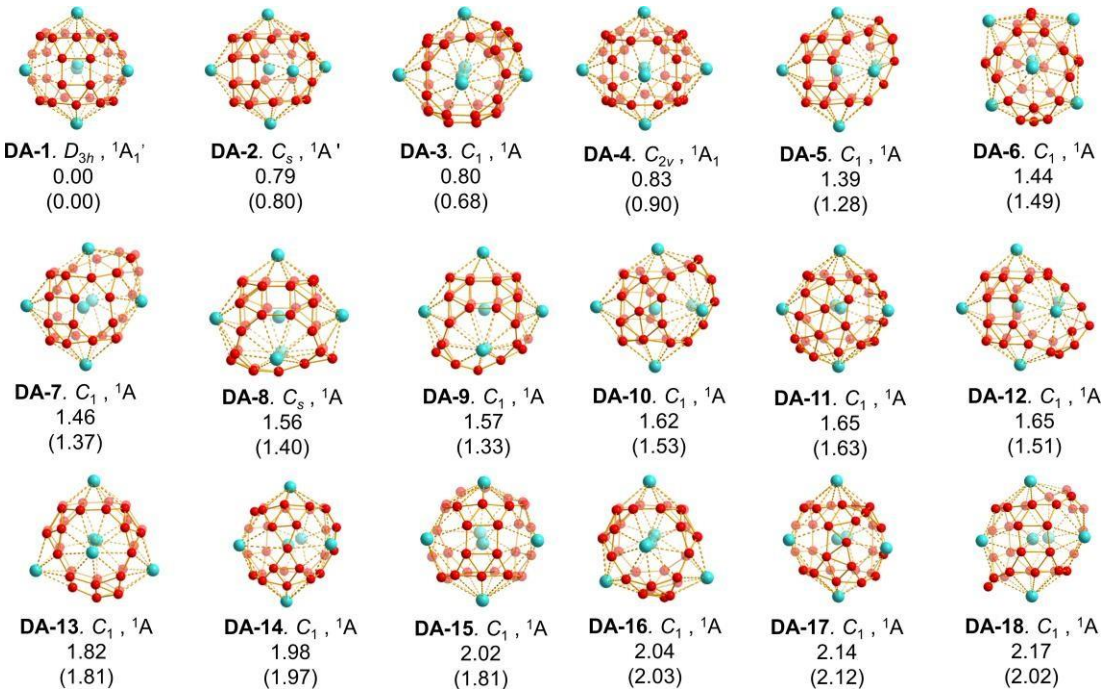

Figure S4. Eigenvalue spectra of La@[La_5&B_{30}] (**1**) (left) and La@[La_5&B_{30}]$^{2-}$ (**3**) (right) at PBE0/B/6-311+G(d)/La/ECP46MWB level, with the HOMO-LUMO energy gaps indicated in eV.

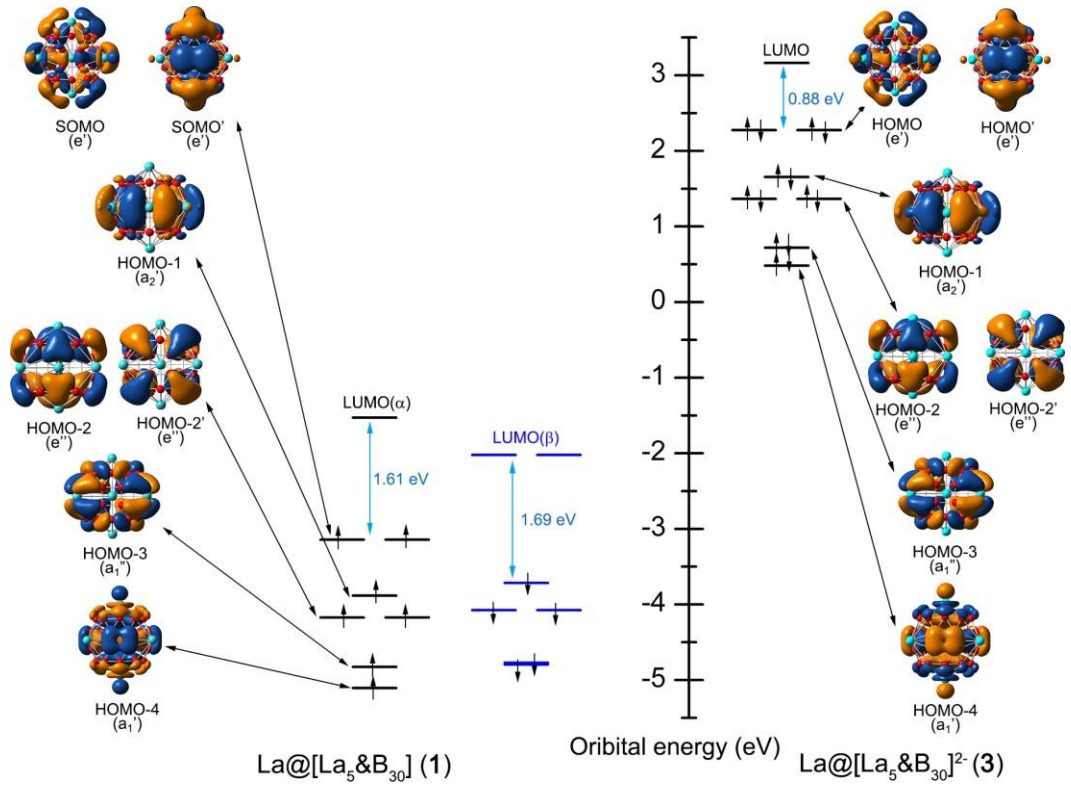

Figure S5. Gibbs free energies **Δ**G_f (eV) of the four lowest-lying isomers of La_6B_{30} at PBE0/B/6-311+G(d)/La/ECP46MWB level as a function of temperature between 0 to 400 K relative to D_{3h} La@[La_5&B_{30}] (**1**) (**NE-1**).

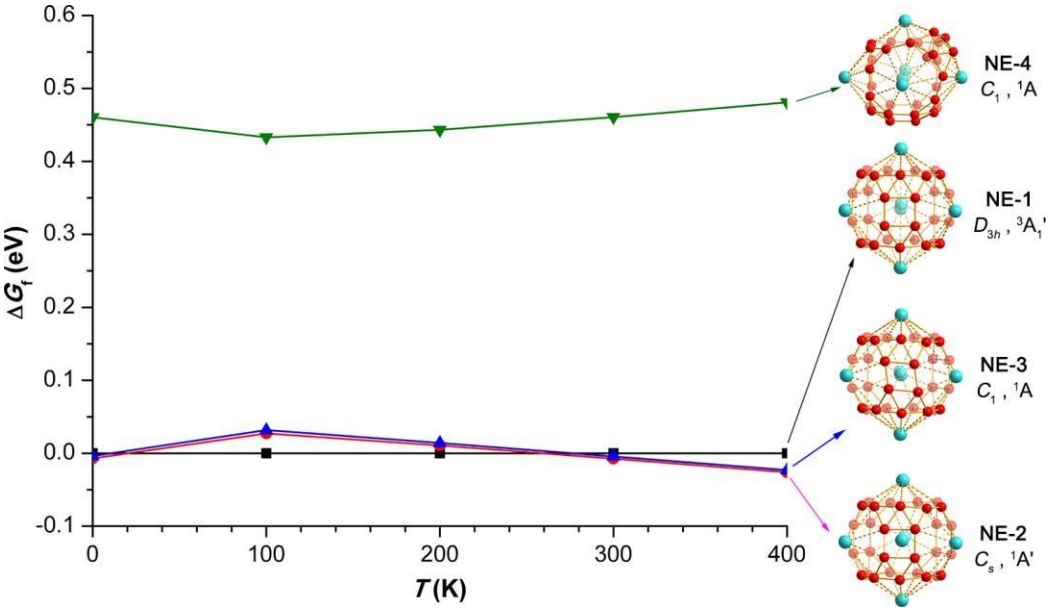

Figure S6. Gibbs free energies ΔG_f (eV) of the four lowest-lying isomers of $La@B_{30}^-$ at PBE0/B/6-311+G(d)/La/ECP46MWB level as a function of temperature between 0 to 400 K relative to C_s $La@[La_5\&B_{30}]^-$ (**2**) (**MA-1**).

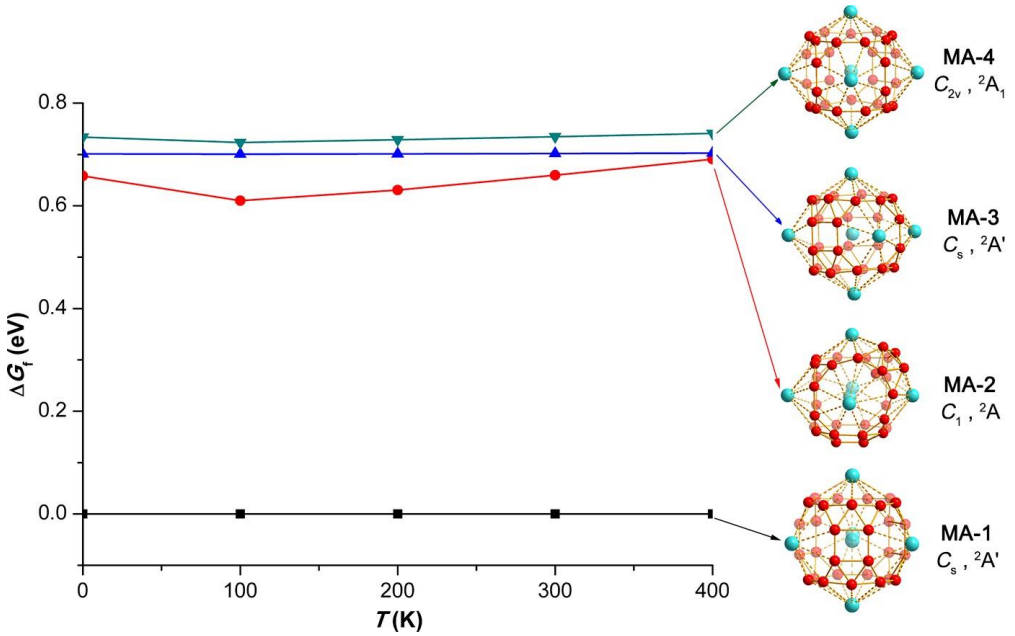

Figure S7. Gibbs free energies ΔG_f (eV) of the four lowest-lying isomers of $La_5B_{30}^-$ at PBE0/B/6-311+G(d)/La/ECP46MWB level as a function of temperature between 0 to 400 K relative to D_{3h} D_{3h} La@$[La_5\&B_{30}]^{2-}$ (**3**) (**DA-1**)..

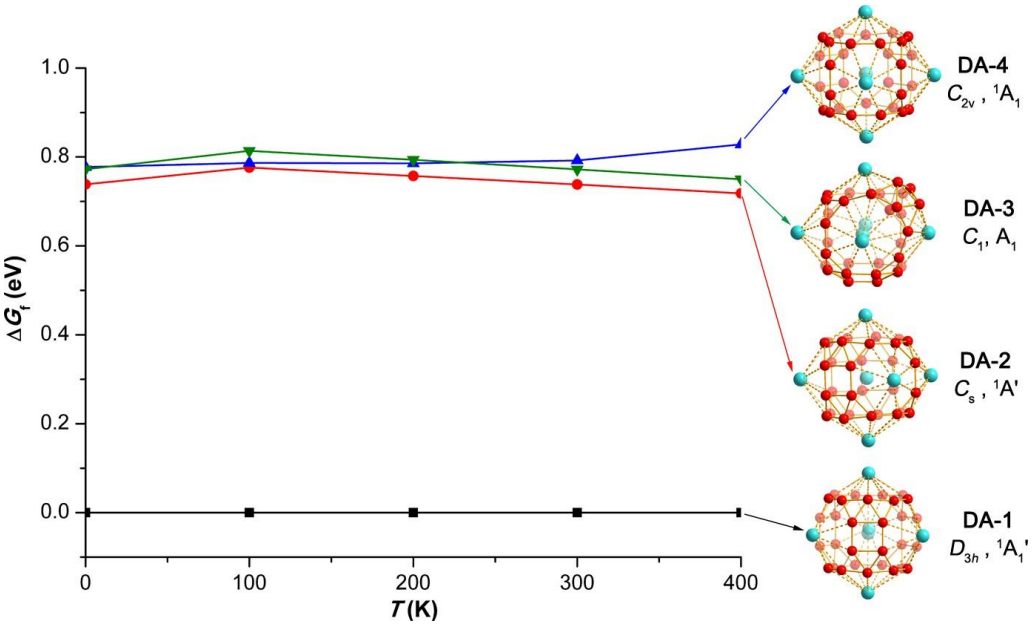

Figure S8. MD simulations of D_{3h} La@[La_5&B_{30}] (**1**) at 1000 K. The calculated root-mean-square-deviation (RMSD) and maximum bond length deviation (MAXD) values (on average) are indicated in Å.

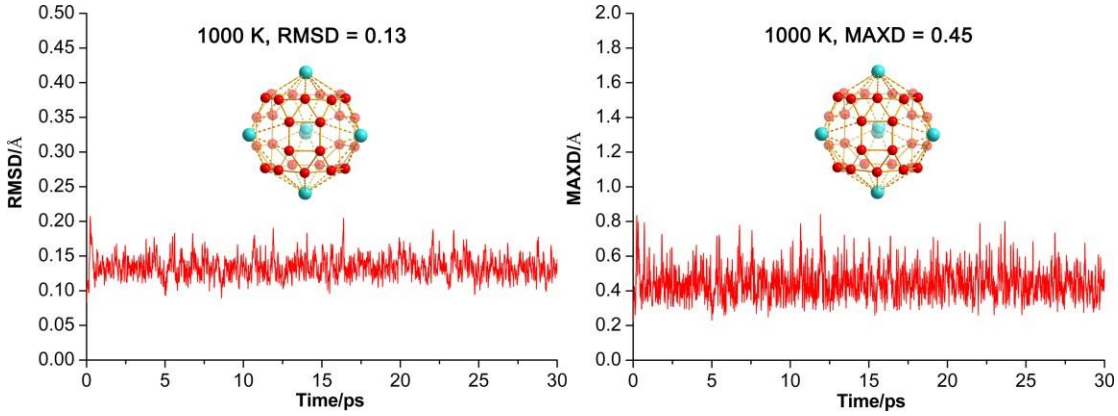

Figure S9. MD simulations of D_{3h} La@[La_5&B_{30}]$^{2-}$ (**3**) at 1000 K. The calculated root-mean-square-deviation (RMSD) and maximum bond length deviation (MAXD) values (on average) are indicated in Å.

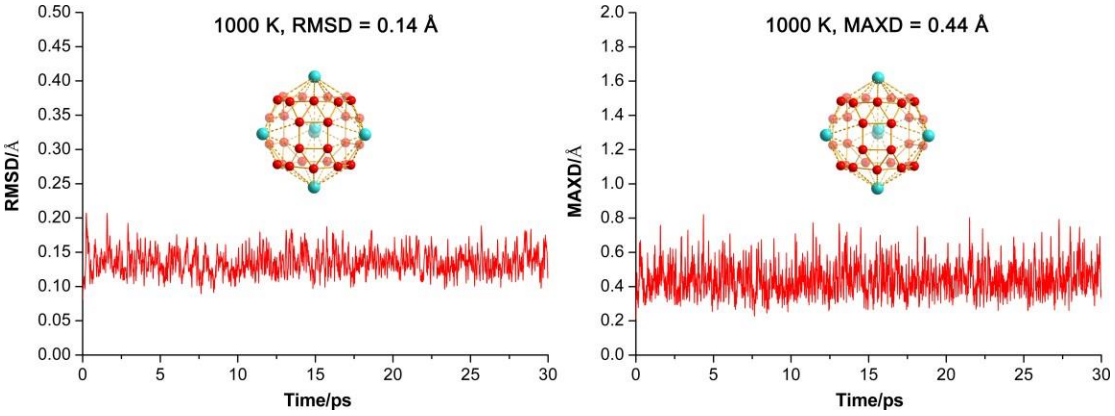

Figure S10. The phonon dispersion frequencies of 1D La_4B_{21} (**4**) nanowire.

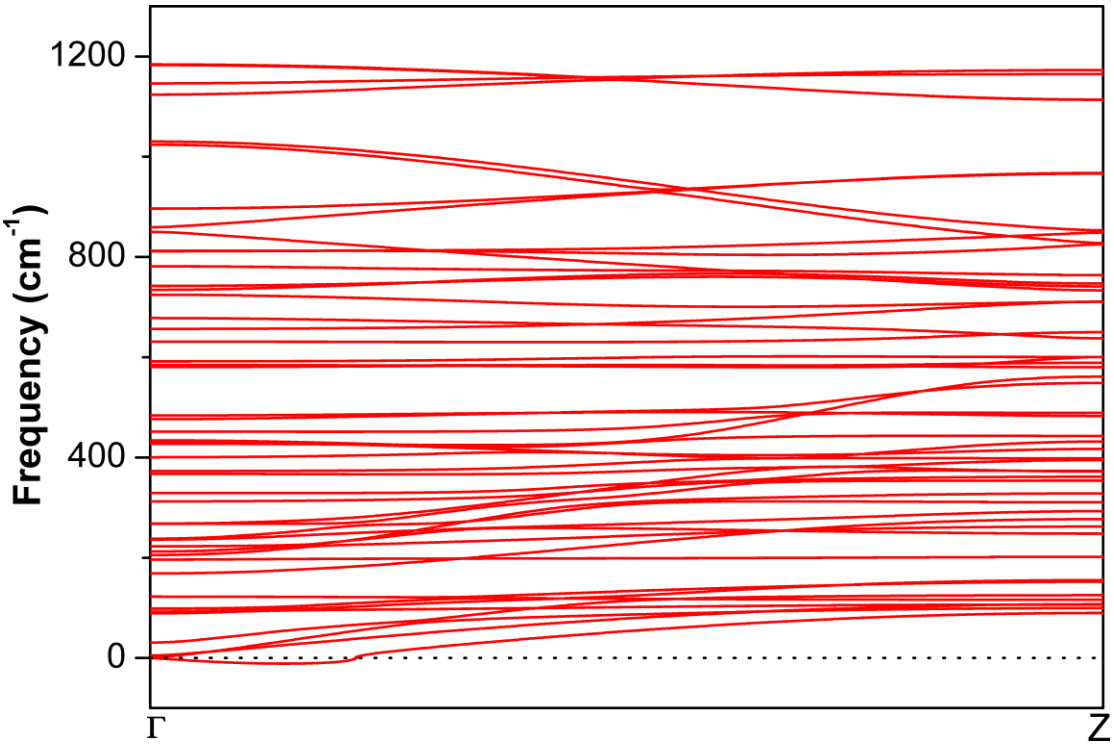

Figure S11. Band structure and projected density of states (PDOS) of 1D La_4B_{21} (**4**) nanowire at PBE level.

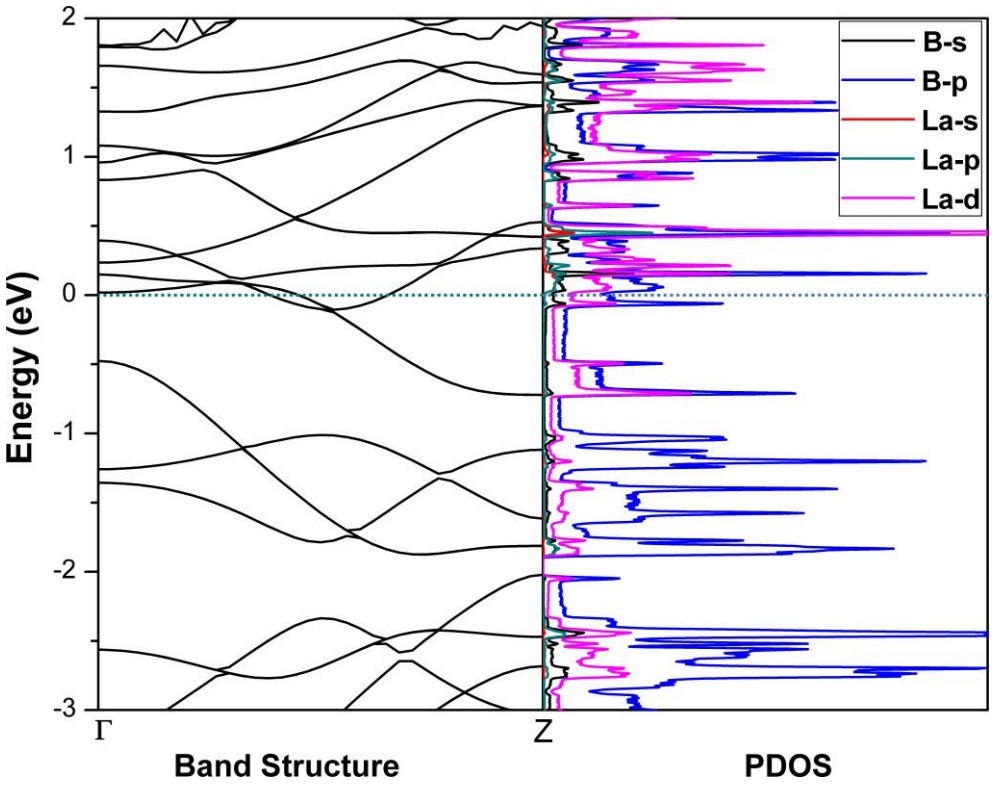

Figure S12. Side and top views of the ico-chemical shielding surfaces (ICSSs) of (a) La@[La_5&B_{30}]$^-$ (**2**), and (b) C_6H_6 based on their calculated NICS-ZZ components. Yellow and green regions stand for chemical shielding and de-shielding areas, respectively.

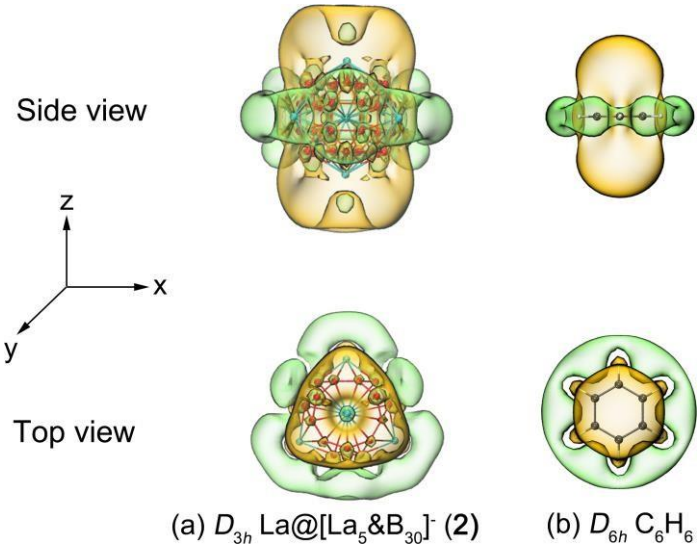

Table S1. Optimized coordinates (x, y, z) of D_{3h} La@[La_5&B_{30}] (**1**, $^3A_1'$) at PBE0/B/6-311+G(d)/La/ECP46MWB level.

B	0.80453200	2.24843100	2.06020900
B	1.96768200	2.18501300	-0.84226200
B	-0.80453200	2.24843100	2.06020900
B	2.87611800	0.61155600	0.84226200
B	-2.87611800	0.61155600	-0.84226200
B	1.96768200	2.18501300	0.84226200
B	2.03308900	1.17380500	2.16656900
B	-1.96768200	2.18501300	0.84226200
B	-2.03308900	1.17380500	2.16656900
La	0.00000000	3.77530500	0.00000000
B	-1.96768200	2.18501300	-0.84226200
B	-2.87611800	0.61155600	0.84226200
B	-0.80453200	2.24843100	-2.06020900
B	-2.03308900	1.17380500	-2.16656900
B	0.80453200	2.24843100	-2.06020900
B	2.03308900	1.17380500	-2.16656900
B	2.87611800	0.61155600	-0.84226200
La	0.00000000	0.00000000	0.00000000
B	0.90843600	-2.79656900	-0.84226200
B	2.34946400	-0.42747000	-2.06020900
B	1.54493200	-1.82096100	-2.06020900
B	1.54493200	-1.82096100	2.06020900
La	3.26951000	-1.88765300	0.00000000
B	2.34946400	-0.42747000	2.06020900
B	-2.34946400	-0.42747000	2.06020900
B	-0.90843600	-2.79656900	-0.84226200
B	-1.54493200	-1.82096100	2.06020900
B	-1.54493200	-1.82096100	-2.06020900
La	-3.26951000	-1.88765300	0.00000000
B	-2.34946400	-0.42747000	-2.06020900
B	-0.90843600	-2.79656900	0.84226200
B	0.90843600	-2.79656900	0.84226200
B	0.00000000	-2.34760900	2.16656900
B	0.00000000	-2.34760900	-2.16656900
La	0.00000000	0.00000000	3.53305600
La	0.00000000	0.00000000	-3.53305600

Table S2. Optimized coordinates (x, y, z) of C_s La@[La_5&B_{30}]$^-$ (**2**, ^{2}A') at PBE0/B/6-311+G(d)/La/ECP46MWB level.

B	-1.51491900	1.84955300	2.07573600
B	-0.85894500	2.80011800	-0.84235400
B	-2.36025300	0.47576800	2.10446200
B	0.96912700	2.76389900	0.84222000
B	-2.02709000	-2.12958900	-0.84306500
B	-0.85894500	2.80011800	0.84235400
B	0.04635600	2.34630600	2.16927300
B	-2.88068100	-0.53953000	0.83477900
B	-2.06331600	-1.12492700	2.18808300
La	-3.22679800	1.93473700	0.00000000
B	-2.88068100	-0.53953000	-0.83477900
B	-2.02709000	-2.12958900	0.84306500
B	-2.36025300	0.47576800	-2.10446200
B	-2.06331600	-1.12492700	-2.18808300
B	-1.51491900	1.84955300	-2.07573600
B	0.04635600	2.34630600	-2.16927300
B	0.96912700	2.76389900	-0.84222000
La	0.00207200	0.00534900	0.00000000
B	2.85700800	-0.65165100	-0.83483800
B	1.58690900	1.78895800	-2.07651900
B	2.37703700	0.38287700	-2.10435200
B	2.37703700	0.38287700	2.10435200
La	3.30112000	1.80717700	0.00000000
B	1.58690900	1.78895800	2.07651900
B	-0.85359100	-2.21918000	2.06118400
B	1.94093600	-2.20788300	-0.84320800
B	0.76460200	-2.25069600	2.06072200
B	0.76460200	-2.25069600	-2.06072200
La	-0.07437400	-3.73931700	0.00000000
B	-0.85359100	-2.21918000	-2.06118400
B	1.94093600	-2.20788300	0.84320800
B	2.85700800	-0.65165100	0.83483800
B	2.01662800	-1.20477400	2.18723800
B	2.01662800	-1.20477400	-2.18723800
La	-0.00099300	-0.01092500	3.51812300
La	-0.00099300	-0.01092500	-3.51812300

Table S3. Optimized coordinates (x, y, z) of D_{3h} La@[La_5&B_{30}]$^{2-}$ (**3**, $^1A_1'$) at PBE0/B/6-311+G(d)/La/ECP46MWB level.

B	0.81051700	2.25761800	2.10126100
B	1.95664700	2.17472300	-0.83886500
B	-0.81051700	2.25761800	2.10126100
B	2.86168900	0.60714400	0.83886500
B	-2.86168900	0.60714400	-0.83886500
B	1.95664700	2.17472300	0.83886500
B	2.03288600	1.17368700	2.19463100
B	-1.95664700	2.17472300	0.83886500
B	-2.03288600	1.17368700	2.19463100
La	0.00000000	3.74001400	0.00000000
B	-1.95664700	2.17472300	-0.83886500
B	-2.86168900	0.60714400	0.83886500
B	-0.81051700	2.25761800	-2.10126100
B	-2.03288600	1.17368700	-2.19463100
B	0.81051700	2.25761800	-2.10126100
B	2.03288600	1.17368700	-2.19463100
B	2.86168900	0.60714400	-0.83886500
La	0.00000000	0.00000000	0.00000000
B	0.90504200	-2.78186700	-0.83886500
B	2.36041300	-0.42688000	-2.10126100
B	1.54989600	-1.83073700	-2.10126100
B	1.54989600	-1.83073700	2.10126100
La	3.23894700	-1.87000700	0.00000000
B	2.36041300	-0.42688000	2.10126100
B	-2.36041300	-0.42688000	2.10126100
B	-0.90504200	-2.78186700	-0.83886500
B	-1.54989600	-1.83073700	2.10126100
B	-1.54989600	-1.83073700	-2.10126100
La	-3.23894700	-1.87000700	0.00000000
B	-2.36041300	-0.42688000	-2.10126100
B	-0.90504200	-2.78186700	0.83886500
B	0.90504200	-2.78186700	0.83886500
B	0.00000000	-2.34737500	2.19463100
B	0.00000000	-2.34737500	-2.19463100
La	0.00000000	0.00000000	3.51110500
La	0.00000000	0.00000000	-3.51110500

Table S4. Optimized fractional coordinates (x, y, z) of 1D La_4B_{21} (**4**) nanowire at PBE level.

34.7623263024369464 -0.0037103936372768 0.0053697325008126
-17.3843731436830922 30.1100482126263138 -0.0048079227471372
0.0006665636019442 -0.0003024596182199 4.4370652451652273
B La
21 4
0.5224592918596261 0.6254264817409362 0.9896625959311190
0.5522889666654875 0.6295724703335202 0.3104362083764923
0.5867764599825427 0.6024999529082078 0.6777937495049429
0.4029085946912579 0.5080085721366879 0.3104998036490051
0.5551323717812721 0.6331372921064196 0.6779315518371957
0.5614496737495117 0.6082124069822457 0.9911003439693392
0.4299967408886526 0.5695721242593303 0.6780707112541254
0.4242755949154859 0.5385337797565303 0.9912531868984529
0.4328811473290442 0.5689206417184052 0.3105651242709059
0.3993514661695243 0.5072921559289154 0.6779981600363576
0.5832398189599132 0.5996114872801365 0.3102970815834436
0.5244796270251985 0.4802147829537784 0.3101917285681349
0.5796829356167068 0.5700187746029498 0.9894281524889664
0.4070568630640384 0.4823312198332277 0.9896230238753436
0.4635655661245760 0.4492694479351648 0.3102856910611972
0.4375169966203097 0.4528198302592091 0.9895251385930619
0.4629121992173481 0.4457306194052912 0.6777742060423625
0.5251955306799815 0.4773712749845935 0.6776847603365015
0.4939506549782170 0.4710488828293640 0.9909858796693893
0.4624780233080154 0.5949632089173467 0.9897244507077025
0.5501634821723542 0.5100432719650027 0.9893759743163675
0.4920645556303757 0.6481555363748028 0.4915080451662049
0.4932284716647780 0.5392686809017450 0.6127949791951457
0.6032993172071554 0.5404415810714001 0.4910618641458554
0.3843153736986520 0.4292051288147651 0.4913377935223999